REPORT

PHYSICS

Quantum amplification of mechanical oscillator motion

S. C. Burd[1,2]*, R. Srinivas[1,2], J. J. Bollinger[1], A. C. Wilson[1], D. J. Wineland[1,2,3], D. Leibfried[1], D. H. Slichter[1], D. T. C. Allcock[1,2,3]

Detection of the weakest forces in nature is aided by increasingly sensitive measurements of the motion of mechanical oscillators. However, the attainable knowledge of an oscillator's motion is limited by quantum fluctuations that exist even if the oscillator is in its lowest possible energy state. We demonstrate a technique for amplifying coherent displacements of a mechanical oscillator with initial magnitudes well below these zero-point fluctuations. When applying two orthogonal squeezing interactions, one before and one after a small displacement, the displacement is amplified, ideally with no added quantum noise. We implemented this protocol with a trapped-ion mechanical oscillator and determined an increase by a factor of up to 7.3 (±0.3) in sensitivity to small displacements.

Mechanical oscillators are essential components in an increasing variety of precision sensing applications, including gravitational wave detection (*1*), atomic force microscopy (*2*), cavity optomechanics (*3*), and measurement of weak electric fields (*4*). Quantum mechanically, any harmonic oscillator can be described by a pair of noncommuting observables; for a mechanical oscillator, these are typically position and momentum. The precision of measurement of these observables is limited by unavoidable quantum fluctuations that are present even if the oscillator is in its ground state. Using the method of "squeezing," these zero-point fluctuations can be manipulated while preserving their product as dictated by the Heisenberg uncertainty relation. This squeezing allows for improved measurement precision for one observable at the expense of increased fluctuations in the other (*5*).

Although squeezed states have been created in a variety of physical systems, including electromagnetic fields (*6*), spin systems (*7*), micromechanical oscillators (*8*–*10*), and the motional modes of single trapped ions (*11*, *12*), exploiting squeezing for enhanced metrology has been challenging. In particular, noise added during the detection process will limit the metrological enhancement unless it is smaller than the squeezed noise. The requirement of low-noise detection can be overcome by increasing the magnitude of the signal to be measured. In optical interferometry (*13*) and in spin systems (*14*), it has been shown that reversal of squeezing interactions can magnify small phase shifts, thereby relaxing detection requirements (*15*). Photon field displacements in microwave cavities have also been amplified using similar phase-sensitive amplification schemes (*16*, *17*). However, in mechanical oscillator systems, technical challenges in implementing reversible squeezing interactions have prevented prior use of such methods.

We present a protocol, based on reversible squeezing, for ideally noiseless phase-sensitive amplification (*5*) of mechanical oscillator displacements. This amplification method (Fig. 1) is applicable to any harmonic oscillator where reversible squeezing can be implemented faster than system decoherence. By first squeezing the motional ground state, quantum fluctuations along a particular phase space quadrature are suppressed. A small initial displacement α_i (to be amplified) is then applied along the squeezed axis. At this stage, although the signal-to-noise ratio (SNR) for measuring α_i has been improved by squeezing, resolution below the zero-point fluctuations would require a detection method with yet lower noise. Finally, by reversing the squeezing interaction, the oscillator returns to a minimum-uncertainty coherent state with a larger amplitude $\alpha_f = G\alpha_i$, where G is the gain. Ideally, this process adds no noise in either quadrature. For an oscillator described using creation and annihilation operators $\hat{a}^\dagger$ and $\hat{a}$, the amplification is given by the identity

$$\hat{D}(\alpha_f) = \hat{S}^\dagger(\xi)\hat{D}(\alpha_i)\hat{S}(\xi) \quad (1)$$

(*18*), where $\hat{D}(\alpha) = \exp(\alpha\hat{a}^\dagger - \alpha^*\hat{a})$ is the displacement operator, and $\hat{S}(\xi) = \exp[(\xi^*\hat{a}^2 - \xi\hat{a}^{\dagger 2})/2]$ is the squeezing operator with complex squeezing parameter $\xi(r, \theta) = r\exp(i\theta)$. For arbitrary orientations of the displacement α_i with respect to the initial squeezing axis, $\alpha_f = \alpha_i\cosh(r) + \alpha_i^*\exp(i\theta)\sinh(r)$. Maximum amplification is achieved if the displacement is along the squeezed axis where $\arg(\alpha_i) = \theta/2$, giving $G = \exp(r)$.

We demonstrate this technique using a single trapped $^{25}Mg^+$ ion as the mechanical oscillator (*19*). The ion is held ~30 μm above a linear surface-electrode radio-frequency trap (*20*, *21*), which is cryogenically cooled to 18 K. Experiments are performed on a radial motional mode of the ion with frequency $\omega_r \approx 2\pi \times 6.3$ MHz, energy eigenstates denoted by $|n\rangle$, and zero-point wave function extent of ~5.7 nm (*19*). To analyze the motional state, we use qubit states $|\downarrow\rangle \equiv |F = 3, m_F = 1\rangle$ and $|\uparrow\rangle \equiv |F = 2, m_F = 1\rangle$ within the $^2S_{1/2}$ electronic ground-state hyperfine manifold, where F is the total angular momentum and m_F is its projection along the direction of the quantization magnetic field of approximately 21.3 mT. The qubit transition frequency $\omega_0 \approx 2\pi \times 1.686$ GHz is first-order insensitive to magnetic field fluctuations, giving a qubit coherence time longer than 200 ms (*21*). The qubit state can be manipulated with resonant microwave carrier pulses. In each experiment, the ion is initialized in the electronic and motional ground state $|\downarrow\rangle|0\rangle$ with optical pumping, resolved-sideband laser cooling (*22*), and microwave pulses. Qubit readout is accomplished by applying a laser resonant with the $^2S_{1/2} \leftrightarrow {}^2P_{3/2}$ cycling transition and detecting state-dependent ion fluorescence. We analyze the motional state of the ion by applying sideband interactions to map it onto the qubit states (*11*, *12*). Applying a sideband interaction for various durations results in qubit Rabi oscillations with multiple frequency components whose amplitudes depend on the Fock state populations. We generate these

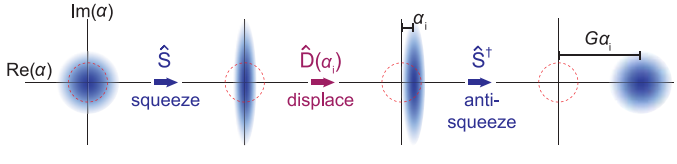

Fig. 1. Conceptual illustration of the amplification protocol. Each panel shows a Wigner function phase space distribution (not to scale) in a frame rotating at the oscillator frequency. A displacement α_i of an initially squeezed ground state is amplified by subsequent reversed squeezing ("anti-squeezing"), resulting in a final coherent state with amplitude $G\alpha_i$ with no added noise. Dashed red circles indicate the characteristic extent of the initial ground-state fluctuations.

[1]Time and Frequency Division, National Institute of Standards and Technology, Boulder, CO 80305, USA. [2]Department of Physics, University of Colorado, Boulder, CO 80309, USA. [3]Department of Physics, University of Oregon, Eugene, OR 97403, USA.
*Corresponding author. Email: shaun.burd@colorado.edu

interactions using oscillating magnetic field gradients (*21*). The blue sideband (BSB) interaction induces transitions between the states $|\downarrow\rangle|n\rangle$ and $|\uparrow\rangle|n+1\rangle$ with Rabi frequencies proportional to $\sqrt{n+1}$. The red sideband (RSB) interaction drives transitions between $|\downarrow\rangle|n\rangle$ and $|\uparrow\rangle|n-1\rangle$ with Rabi frequencies proportional to $\sqrt{n}$ and will not cause a qubit transition if the ion is in $|\downarrow\rangle|0\rangle$.

Squeezing of the motional state is accomplished by applying an oscillating potential at twice the motional frequency ($2\omega_r$) to the radio-frequency electrodes of the trap (*23*). This modulates the confining potential for the ion, yielding the interaction picture Hamiltonian

$$\hat{H} = i\hbar\frac{g}{2}\left[\hat{a}^2\exp(-i\theta) - \hat{a}^{\dagger 2}\exp(i\theta)\right] \quad (2)$$

(*19*), where $\hbar$ is the Planck constant divided by 2π, g is the parametric coupling strength, and θ is the phase of the parametric modulation. Applying this Hamiltonian for duration t implements the unitary squeezing operator $\hat{S}(\xi)$ with $r = gt$. Although electronic parametric modulation has been used with single ions to squeeze a thermal state of motion (*24*) and for phase-sensitive parametric amplification of highly displaced thermal states (*25*), it has not previously been implemented on pure quantum states. Optical forces can also be used for parametric modulation (*11*), but decoherence due to photon scattering and higher-order nonlinearities in the optical field have limited the achievable squeezing (*11*). Squeezed mechanical oscillator states can also be prepared using dissipative reservoir engineering (*8*, *12*). However, this is not a unitary squeezing operation, as is required for the amplification method described here.

We characterize our squeezing process using motional sideband analysis to extract Fock state populations (*19*) (Fig. 2). To characterize the unitarity of our squeezing operations, we measure the ground-state population after squeezing and anti-squeezing, $\langle 0|\hat{S}^{\dagger}\hat{S}|0\rangle$. For $r < 2$, this population is ~0.98, which is consistent with the measured value without squeezing and anti-squeezing ($r = 0$). The population in $n = 0$ remains above 0.93 for $r < 2.37$ (±0.03), or 20.6 (±0.3) dB of squeezing (*19*). The calibrated parametric coupling strength is $g = 2\pi \times 50.2$ (±0.2) kHz, equivalent to a squeezing rate of 2.75 (±0.02) dB/μs.

We use this unitary squeezing interaction to demonstrate amplification of harmonic oscillator displacements (see Fig. 1). Displacements are implemented by applying an oscillating potential resonant with the motional mode (at frequency ω_r) to an electrode of the ion trap (*19*). All control fields are digitally synthesized with the same reference clock, enabling stable and deterministic control of the relative phases between the displacement, squeezing, sideband, and carrier interactions. At each stage of the amplification process, we verify the Fock state composition of the ion's motional state using sideband analysis (Fig. 2, A to C). The measured gain for various values of the squeezing parameter closely follows the theoretically expected exponential growth of the coherent state amplitude (Fig. 2E).

Using this amplification technique, we achieve increased sensitivity when measuring displacements much smaller than the zero-point fluctuations. To map the final displacements α_f onto the qubit states, we use a phase-sensitive red sideband (PSRSB) method (*26*) (Fig. 3A), which reaches the standard quantum limit for $|\alpha_f| \ll 1$ (*19*). Here, a displacement of the motional ground state results in a probability of measuring $|\downarrow\rangle$ of $P_{\downarrow} = \frac{1}{2}[1 - C(|\alpha_f|)\cos\phi]$, where $C(|\alpha_f|)$ is the signal contrast and ϕ is the phase of a carrier $\pi/2$ pulse, which follows the RSB π mapping pulse. For $|\alpha_f| \ll 1$, $C(\alpha_f) \approx 2|\alpha_f|$. In comparison, simply measuring the qubit directly after the RSB π pulse gives a signal $P_{\downarrow} \propto |\alpha_f|^2$. Without amplification, $\alpha_f = \alpha_i$ and the PSRSB contrast is $C(|\alpha_i|)$. With amplification, the initial displacement amplitude α_i is ideally increased by a factor of G and the PSRSB contrast becomes $C(|G\alpha_i|)$. This increase in contrast is shown in Fig. 3B, where the presence of oscillations for the state after amplification indicates that it has a well-defined motional phase. The carrier phase dependence in this figure is a feature of the PSRSB method, not of the amplification protocol. Figure 3C highlights the phase-sensitive nature of the amplification protocol by plotting the contrast C of the PSRSB fringe against the squeezing phase θ for a fixed displacement. Maximum amplification is achieved when the displacement is oriented along the squeezed axis of the initial squeezed state in motional phase space (see Fig. 1). Figure 3D shows the measured signal contrast as a function of $|\alpha_i|$ for various parametric drive durations. For each displacement, the contrast is defined as $C \equiv P_{\downarrow,\max} - P_{\downarrow,\min}$, where $P_{\downarrow,\max}$ and $P_{\downarrow,\min}$ are the maximum and minimum, respectively, of the fringes shown in Fig. 3B. The uncertainty in measuring the contrast is $\sigma(C) = \sqrt{\sigma(P_{\downarrow,\max})^2 + \sigma(P_{\downarrow,\min})^2}$, where $\sigma(P_{\downarrow,\max(\min)})^2$ is the variance of the projection noise associated with measuring $P_{\downarrow,\max(\min)}$. The SNR for a displacement measurement is then $s(G) = C(G\alpha_i)/\sigma[C(G\alpha_i)]$. For a given number of experiments, amplification allows the SNR for a displacement measurement to be improved in comparison to the ideal PSRSB measurement with no squeezing (Fig. 3D, black solid line), giving a measurement sensitivity enhancement of $s(G)/s(G = 1)$. For measurements where $C \lesssim 0.25$, the contrast varies linearly with $|\alpha_i|$, and the gain in contrast $C(G\alpha_i)/C(\alpha_i)$ sets a lower bound (which becomes exact as $|\alpha_i| \to 0$) on the measurement sensitivity enhancement, because the projection noise decreases monotonically with increasing contrast. Increasing the squeezing results in increased contrast for $|\alpha_f| \ll 1$, up to a squeezing time of approximately 8 μs [corresponding to $r = 2.54$

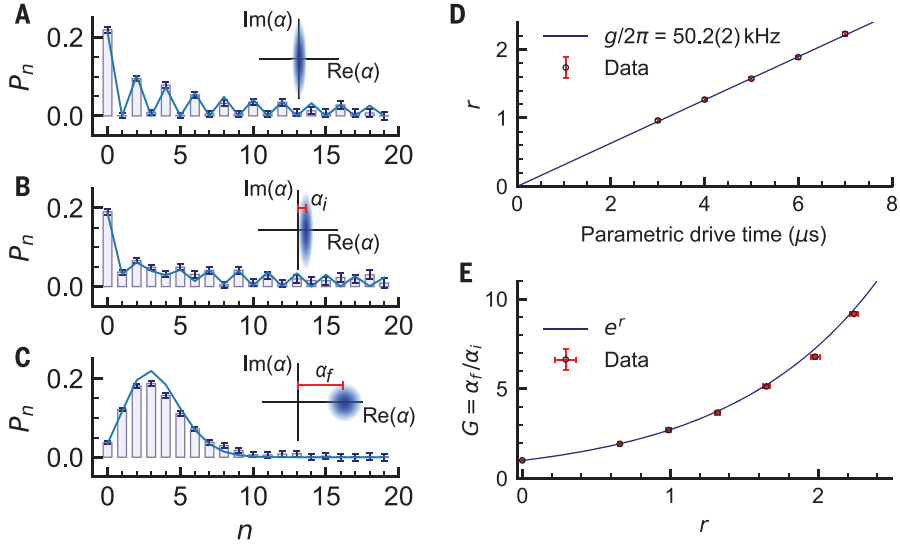

Fig. 2. Fock state population analysis. (**A** to **C**) Histograms of Fock state populations extracted by fitting to BSB Rabi oscillations. Vertical bars are derived by fitting to an unconstrained population distribution. Solid blue lines are fits assuming parameterized functional forms of the ideal Fock state populations, yielding values of r, α_i, and α_f (*19*). Insets show Wigner function illustrations of the corresponding motional states. (A) Initial squeezed motional ground state with $r = 2.26$ (±0.02). (B) After displacing this state by $\alpha_i = 0.200$ (±0.002). (C) Final coherent state with amplitude $\alpha_f = 1.83$ (±0.01), following the reversed squeezing operation. The initial displacement is amplified by $G = \alpha_f/\alpha_i = 9.17$ (±0.09). (**D**) Squeezing parameter r (black circles) as a function of the parametric drive duration. The solid line is a linear fit whose slope gives the parametric coupling strength g. (**E**) Measured gain (black circles) as a function of the squeezing parameter r. The solid line is the theoretical gain $G = \exp(r)$. Error bars denote SD.

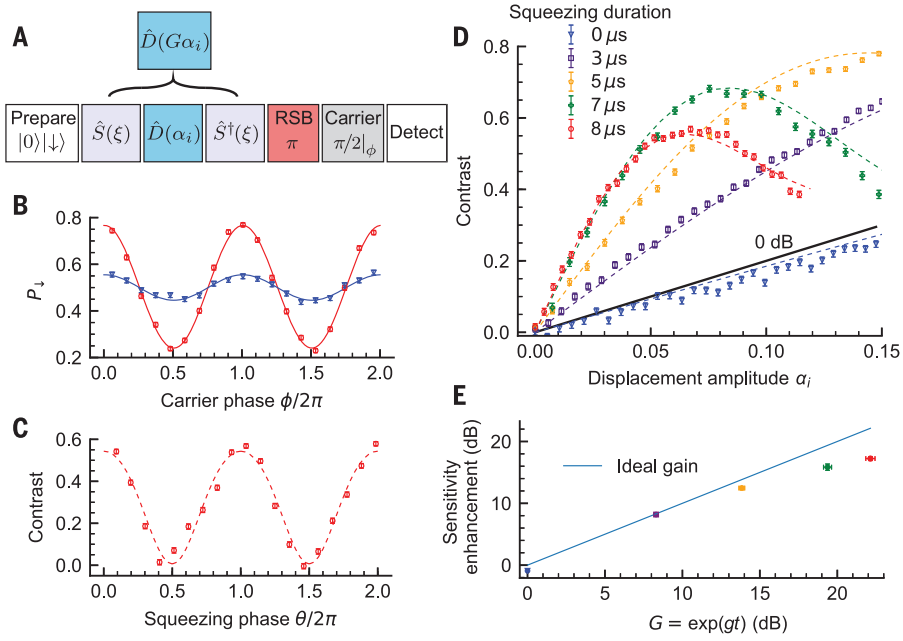

Fig. 3. Measurement sensitivity enhancement. (**A**) Pulse sequence for displacement sensing protocol with PSRSB detection. (**B**) Population in $|\downarrow\rangle$ as a function of the carrier $\pi/2$ pulse phase. Blue inverted triangles, data with no squeezing; red circles, data with amplification. Solid lines show sinusoidal fits to the data. (**C**) Contrast of the carrier phase scan, as shown in (B), as a function of the squeezing phase θ for a fixed displacement. (**D**) Contrast as a function of the displacement amplitude $|\alpha_i|$ for different initial squeezing pulse durations. Each data point is calculated from ~10^4 experiments. The data shown in (B) and (C) have initial $|\alpha_i| = 0.0578$ (±0.0006) and a squeezing duration of $t = 8$ μs [nominally $r = 2.54$ (±0.03)]. The solid black line in (D) is the maximum theoretical contrast without squeezing. Dashed lines in (C) and (D) are derived from a numerical model that includes motional decoherence. (**E**) Measurement sensitivity enhancement in the linear small-displacement regime as a function of the ideal gain $G = \exp(gt)$. For each squeezing duration, the enhancement is determined by dividing the slope of the contrast for $C \lesssim 0.25$ [obtained by fitting a straight line to data points in (D) with $C \lesssim 0.25$] by the slope of the 0 dB black line, which represents the standard quantum limit (*19*). Error bars denote SD.

(±0.03), and ideally 22.0 (±0.3) dB of squeezing]. Here, we achieved a contrast gain of 7.3 (±0.3), corresponding to a factor of 53 (±4) reduction in the number of measurements required to achieve a given SNR, equivalent to a 17.2 (±0.3) dB enhancement in measurement sensitivity. For larger squeezing durations, degradation of the contrast due to background motional heating and dephasing in our trap prevents a further increase in gain. This is not a limitation of the amplification process or our squeezing method. We note that with amplification, we can achieve a SNR of 1 for measuring a displacement of one Bohr radius (~0.0529 nm, corresponding to $\alpha \approx 0.00467$), less than the extent of the ground-state vacuum fluctuations ($\alpha = 0.5$) by a factor of 107, in ~200 experiments.

We have implemented a fast unitary squeezing interaction in a simple mechanical oscillator and used it to amplify and detect coherent motional displacements that are significantly smaller than the quantum zero-point fluctuations. This amplification technique can enhance measurement sensitivity in protocols that use phase-stable displacements, such as photon-recoil spectroscopy (*26*, *27*), where the phase of momentum kicks from photon absorption can be controlled by modulating the photon source. Our method can be extended to amplify displacements of unknown frequency or phase, following the recent proposal in (*28*). The parametric modulation used for squeezing can also be combined with a spin-dependent force to enhance phonon-mediated spin-spin interactions (*28*, *29*), which are used to create entanglement in quantum simulation and quantum information processing experiments. Our methods are also applicable to the generation of exotic nonclassical motional states and to continuous-variable quantum information processing (*30*). Finally, we note that the squeezing, displacement, spin-motion coupling, and qubit control interactions used in this work are all generated without lasers, thereby eliminating spontaneous emission, simplifying control of relative phases, and enabling use with other charged particles lacking optical transitions such as electrons, positrons, and (anti-)protons (*23*).

REFERENCES AND NOTES

1. LIGO Scientific Collaboration and Virgo Collaboration, *Phys. Rev. Lett.* **116**, 061102 (2016).
2. H.-J. Butt, B. Cappella, M. Kappl, *Surf. Sci. Rep.* **59**, 1–152 (2005).
3. M. Aspelmeyer, T. J. Kippenberg, F. Marquardt, *Rev. Mod. Phys.* **86**, 1391–1452 (2014).
4. M. J. Biercuk, H. Uys, J. W. Britton, A. P. VanDevender, J. J. Bollinger, *Nat. Nanotechnol.* **5**, 646–650 (2010).
5. C. M. Caves, *Phys. Rev. D* **23**, 1693–1708 (1981).
6. R. E. Slusher, L. W. Hollberg, B. Yurke, J. C. Mertz, J. F. Valley, *Phys. Rev. Lett.* **55**, 2409–2412 (1985).
7. O. Hosten, N. J. Engelsen, R. Krishnakumar, M. A. Kasevich, *Nature* **529**, 505–508 (2016).
8. E. E. Wollman *et al.*, *Science* **349**, 952–955 (2015).
9. F. Lecocq, J. B. Clark, R. W. Simmonds, J. Aumentado, J. D. Teufel, *Phys. Rev. X* **5**, 041037 (2015).
10. J.-M. Pirkkalainen, E. Damskägg, M. Brandt, F. Massel, M. A. Sillanpää, *Phys. Rev. Lett.* **115**, 243601 (2015).
11. D. M. Meekhof, C. Monroe, B. E. King, W. M. Itano, D. J. Wineland, *Phys. Rev. Lett.* **76**, 1796–1799 (1996).
12. D. Kienzler *et al.*, *Science* **347**, 53–56 (2015).
13. B. Yurke, S. L. McCall, J. R. Klauder, *Phys. Rev. A* **33**, 4033–4054 (1986).
14. E. Davis, G. Bentsen, M. Schleier-Smith, *Phys. Rev. Lett.* **116**, 053601 (2016).
15. D. Linnemann *et al.*, *Phys. Rev. Lett.* **117**, 013001 (2016).
16. M. Malnou *et al.*, *Phys. Rev. X* **9**, 021023 (2019).
17. A. Eddins *et al.*, *Phys. Rev. Lett.* **120**, 040505 (2018).
18. M. M. Nieto, D. R. Truax, *Fortschr. Phys.* **45**, 145–156 (1997).
19. See supplementary materials.
20. S. Seidelin *et al.*, *Phys. Rev. Lett.* **96**, 253003 (2006).
21. C. Ospelkaus *et al.*, *Nature* **476**, 181–184 (2011).
22. C. Monroe *et al.*, *Phys. Rev. Lett.* **75**, 4011–4014 (1995).
23. D. J. Heinzen, D. J. Wineland, *Phys. Rev. A* **42**, 2977–2994 (1990).
24. V. Natarajan, F. DiFilippo, D. E. Pritchard, *Phys. Rev. Lett.* **74**, 2855–2858 (1995).
25. N. Yu, H. Dehmelt, W. Nagourney, *J. Appl. Phys.* **73**, 8650–8652 (1993).
26. C. Hempel *et al.*, *Nat. Photonics* **7**, 630–633 (2013).
27. Y. Wan *et al.*, *Nat. Commun.* **5**, 3096 (2014).
28. C. Arenz, D. I. Bondar, D. Burgarth, C. Cormick, H. Rabitz, arXiv:1806.00444 [quant-ph] (1 June 2018).
29. W. Ge *et al.*, *Phys. Rev. Lett.* **122**, 030501 (2019).
30. C. Flühmann *et al.*, *Nature* **566**, 513–517 (2019).
31. S. C. Burd *et al.*, Data for "Quantum amplification of mechanical oscillator motion". NIST Public Data Repository (2019).

ACKNOWLEDGMENTS

We thank W. Ge, D. Kienzler, and D. M. Lucas for stimulating discussions, and S. M. Brewer and S. S. Kotler for helpful comments on the manuscript. These experiments were performed using the ARTIQ control system. This paper is a contribution of NIST and is not subject to U.S. copyright. **Funding:** S.C.B., R.S., and D.T.C.A. are Associates in the Professional Research Experience Program (PREP) operated jointly by NIST and the University of Colorado, Boulder, under award 70NANB18H006 from the U.S. Department of Commerce, National Institute of Standards and Technology. This work was supported by ARO, ONR, and the NIST Quantum Information Program. **Author contributions:** S.C.B. and D.T.C.A. conceived and carried out the experiments with assistance from R.S. and D.H.S.; the squeezing and amplification protocols were developed by S.C.B. and D.T.C.A. in collaboration with J.J.B. and D.J.W.; D.T.C.A., D.H.S., R.S., and S.C.B. designed and built the apparatus; S.C.B. analyzed the data and wrote the manuscript with input from all authors; and D.T.C.A. and D.H.S. supervised all work, with support from D.L., A.C.W., and D.J.W. **Competing interests:** Authors declare no competing interests. **Data and materials availability:** The data from the main text and supplementary materials are available from the NIST Public Data Repository (*31*).

SUPPLEMENTARY MATERIALS

science.sciencemag.org/content/364/6446/1163/suppl/DC1
Supplementary Text
Figs. S1 to S4
References (*32*–*36*)

17 December 2018; accepted 11 April 2019
10.1126/science.aaw2884